Artificial photosynthetic reaction centers coupled to light-harvesting antennas

Pulak Kumar Ghosh, Anatoly Yu. Smirnov, and Franco Nori

Phys. Rev. E **84**, 061138 — Published 22 December 2011

DOI: 10.1103/PhysRevE.84.061138

Artificial photosynthetic reaction centers coupled to light-harvesting antennas

Pulak Kumar Ghosh[1], Anatoly Yu. Smirnov[1,2], and Franco Nori[1,2]

[1] *Advanced Science Institute, RIKEN, Wako-shi, Saitama, 351-0198, Japan*

[2] *Physics Department, The University of Michigan, Ann Arbor, MI 48109-1040, USA*

Abstract

We analyze a theoretical model for energy and electron transfer in an artificial photosynthetic system. The photosystem consists of a molecular triad (i.e., with a donor, a photosensitive unit, and an acceptor) coupled to four accessory light-harvesting antennas pigments. The resonant energy transfer from the antennas to the artificial reaction center (the molecular triad) is here described by the Förster mechanism. We consider two different kinds of arrangements of the accessory light-harvesting pigments around the reaction center. The first arrangement allows direct excitation transfer to the reaction center from all the surrounding pigments. The second configuration transmits energy via a cascade mechanism along a chain of light-harvesting chromophores, where only one chromophore is connected to the reaction center. We show that the artificial photosynthetic system using the cascade energy transfer absorbs photons in a broader wavelength range and converts their energy into electricity with a higher efficiency than the system based on direct couplings between all the antenna chromophores and the reaction center.

I. INTRODUCTION

The reaction centers of natural photosystems are surrounded by a number of accessory light-harvesting complexes [1, 2]. These light-harvesting antennas absorb sunlight photons and deliver their excitation energy to the reaction center, which creates a charge-separated state. The photosystem of green plants is made up of six photosynthetic accessory pigments: carotene, xanthophyll, phaeophytin a, phaeophytin b, chlorophyll a, and chlorophyll b [1]. Each pigment absorbs light in a different range of the solar spectrum. As a result, the antenna complex significantly increases the effective frequency range for the light absorption, resulting in a highly-efficient photocurrent generation.

The efficient performance of natural photosystems motivates researchers to mimic their functions by creating photosynthetic units, which are combined to antenna complexes with artificial reaction centers. For example, a light-harvesting array of metalated porphyrins has been developed in Ref. [3]. This array absorbs light and rapidly transfers the excitation energy to the reaction center, so that the porphyrin (P)–fullerene (C_{60}) charge-separated state, P^+–C_{60}^-, is formed with a quantum yield $\sim 70\%$. Mixed self-assembled monolayers of the ferrocene (Fc)–porphyrin–fullerene molecular triad and the boron dipyrrin (B) dye have been made in Ref. [4, 5] with the goal to examine both energy and electron transfers in the artificial reaction center (Fc–P–C_{60}), coupled to the light-harvesting molecule B. A quantum yield of $\sim 50\%$ for photocurrent production at the wavelength 510 nm and a quantum yield of $\sim 21\%$ at the wavelength 430 nm have been reported [4].

Recently, a more efficient, sophisticated and rigid antenna-reaction system has been designed in Refs. [6, 7]. This system includes three kinds of light-absorbing chromophores: (i) bis (phenylethynyl)anthracene (BPEA), which absorbs around 450 nm wavelength (blue region); (ii) borondipyrromethene (BDPY), having a strong absorption at 513 nm (green region); and (iii) zinc tetraarylporphyrin, which absorbs both at 418 nm and at 598 nm. This study reports $\sim$100% quantum yield for the excitation transfer and $\sim$95 % quantum yield for the generation of the charge-separated state P^+–C_{60}^-.

Theoretical studies of light-induced electron and proton pumping mechanisms [8, 9] can be useful for a better understanding of, and for optimizing light-to-electricity conversion, as well as for developing new and efficient designs of solar cells. Recently we have theoretically analyzed [10] the light-to-electricity energy conversion in a molecular triad (Fc–P–C_{60}) elec-

tronically coupled to conducting leads. It was shown that the Fc–P–C_{60} triad can transform light energy into electricity with a power-conversion efficiency of order of 40%, provided that the connection of the triad to the leads is strong enough. It should be noted, however, that this prototype solar cell absorbs photons with energies in close proximity to the resonant transition of the central porphyrin molecule. Therefore, a major fraction of the sunlight spectrum is not converted to the electrical form by this device.

In this paper we examine a theoretical model for the light-to-electricity energy conversion by a molecular triad, which is surrounded by four additional light-harvesting antenna complexes. We show that this artificial photosystem is able to generate a photocurrent with a quantum yield of the order of 90% (when the reorganization energy for the resonant energy transfer is relatively high) absorbing photons in a wide range (420–670 nm) of the solar spectrum. We consider two different configurations for the antenna complexes: (a) where each light-harvesting molecule is independently connected (by the Förster energy-transfer mechanism) to the central porphyrin (P) molecule of the triad (Fig. 1a); and (b) where the light-harvesting molecules are arranged in a line (Fig. 1b), with only one molecule directly coupled to the porphyrin and with other molecules forming a chain where the energy propagates in a cascade-manner.

Resonant energy transfer in multi-chromophoric light-harvesting complexes has been theoretically studied in Refs. [2, 11–14]. There, a reaction center is modeled phenomenologically as a set of exciton traps. Here we provide a more detailed model of a reaction center, which directly converts light energy to an electric current.

Let us consider a (D-P-A) reaction center surrounded by several (say, four) accessory light-harvesting antennas. A complex comprised of four antenna chromophores attached to the porphyrin-fullerene reaction center have been recently synthesized and investigated in Ref. [15]. Recently a complex comprised of five porphyrin antennas attached to the control unit has been synthesized in Ref. [16]. Note that our theoretical approach can be applied to any number of antenna chromophores coupled to the reaction center. Even with four antennas, many possible configurations of our photosystem could be considered. However, to simplify this analysis, we will now focus on two extreme cases, with somewhat opposite topologies or networks: a well-connected reaction center (directly connected to *all* four accessory light harvesting antennas), and the opposite case where the central reaction center is coupled to *only one* antenna, which is now part of a linear chain. These two

extreme-opposite topologies or networks can be denoted as star-shaped (shown in Fig. 1a) and linear-chain (Fig. 1b), respectively. The star-shaped topology can be implemented in the manner shown in Ref. [16]; whereas for synthesizing the linear-chain antenna complex experimentalists could use to the procedure described in Ref. [15]. In the latter case this is sufficient to create only one-half of the antenna from Ref. [15] containing a chains BPEA $\rightarrow$ BDPY $\rightarrow$ ZnPy $\rightarrow$ RC (see also Refs. [17],[18]).

Our goal is to find the best way to place these accessory antennas, when more energy is transferred from the antennas to the reaction center and more energy is converted to electricity. The two issues considered here are: (1) how to physically arrange antennas around the central reaction center, and also (2) how to arrange these in *energy-space*. The first issue is topological and focuses on the network connectivity in real space: for instance, how many accessory antennas are connected to a central reaction center. The second issue refers to the *energy match* (or mismatch) between neighboring antennas, and between them and the central reaction center. A large energy mismatch between any connected units in the chain would preclude energy transfer between them. This approximate "energy matching" issue between neighboring units is equally important to keep in mind, not just the real-space topological arrangement of the units. We consider antenna complexes consisting of light-absorbing molecules (BPEA, BDPY and porphyrins) with definite resonant energies. These chromophores are extensively used in experiments [6, 7, 15].

Figure 1 shows the connectivity between the different units: star-shaped topology in (a), and linear-chain configuration in (b). Moreover, the colors there represent, very schematically, the energy range where each unit operates optimally. The linear chain shown there has antennas arranged in a way that nearby units operate in approximately similar energy ranges. This energy-matching issue perhaps is not very clear in Fig. 1, even when seen in color. The energy scales are shown far more explicitly in Fig. 2. Figure 2b clearly shows that the linear chain model considered here operates via an energy cascade, or linear chain-reaction. Like a line of falling dominoes, one event triggering the next one, in a sequential manner, with small energy mismatches between successive energy transfer events. As shown in Fig. 2b, the more energetic antenna is located far away from the reaction center, and it is coupled to an antenna with a slightly lower energy, which is coupled to another antenna with an even slightly lower energy, and so on, moving energetically "downhill" along the chain. Thus, the neighboring antennas must be so both in real space, and *also* in "energy space",

to allow for the efficient transfer of energy between them. Thus, "proximity" between units must be in two spaces: real space and energy space.

This article is organized as follows: in Section II we outline a model for the artificial reaction center (molecular triad) coupled to the antenna complex. We briefly describe our mathematical methods in Sec. III. The parameters are listed in Sec. IV. In Sec. V, we numerically solve the master equations and analyze the energy transfer process. Conclusions are presented in Sec. VI. The methods used are described in more details in the online supplementary material.

II. MODEL

We start with a schematic description of the energy and electron transfer processes in an artificial reaction center D–P–A (Donor–Porphyrin–Acceptor) combined with four antenna chromophores: An1, An2, An3, An4 (see Figs. 1a and 1b, showing two different configurations for these antennas: star-shaped configuration in 1a and chain in 1b). The photosensitive molecular triad, D–P–A, is inserted between two electron reservoirs (electrodes) L and R. The donor, D, is coupled to the left lead, L, and the acceptor, A, is connected to the right lead, R. As in Refs. [4, 10], the donor and acceptor molecules (e.g., ferrocene and fullerene), are connected to each other via the photosensitive molecule (porphyrin, P). This molecule is surrounded by four Accessory Light-Harvesting Pigments (ALHP). Figure 1a corresponds to the situation where all pigments are directly coupled to the photosensitive part (P) of the molecular triad. In this "star-shaped" geometric arrangement, all the ALHP can directly transfer excitations to the photosensitive part of the molecular triad. Figure 1b corresponds to the case where the light-harvesting pigments form a chain, which transfers energy where the excitation moves from one pigment to the next one via nearest-neighbor couplings: An4 $\rightarrow$ An3 $\rightarrow$ An2 $\rightarrow$ An1 $\rightarrow$ P. This cascade-like excitation transfer occurs in an energetically-downhill direction, akin a one-dimensional chain reaction or domino-effect.

Figures 2a and 2b present the energy diagrams of the photosystems described in Figs. 1a and 1b, respectively. The electron transfer chain, L$\rightarrow$D$\rightarrow$P$\rightarrow$ P* $\rightarrow$A$\rightarrow$R, is the same for both configurations (a) and (b), and both begin on the left lead, L. The electrochemical potentials of the left (L) and right (R) electron reservoirs are determined by the parameters μ_L and μ_R, with $\mu_R > \mu_L$. Since the energy level E_D of the donor D is lower than the

potential μ_L of the left lead, $E_D < \mu_L$, electrons can move from the L-reservoir to the level D and, afterwards, to the low-lying ground energy level, E_P, of the porphyrin. When absorbing a photon, the electron in the porphyrin molecule jumps from its ground state P to its excited state P*. A subsequent electron transfer from P* to the acceptor A is driven by a negative energy gradient, $(E_A - E_{P^*}) < 0$. In view of the relation: $E_A > \mu_R$, the electron in A is finally transferred to the right, R, electron reservoir. This is the light-induced electron transition in the porphyrin molecule, which results in an energetically-uphill electron flow in both photosynthetic systems (a) and (b).

Even though these systems (a) and (b) have the similar electron-transport chains, their light-harvesting complexes are arranged quite differently. Each of these complexes, An = An1, ..., An4, can be characterized by a ground, E_{An}, and an excited, E_{An^*}, energy levels with an energy difference $\omega_{An} = E_{An^*} - E_{An}$. Hereafter, we assume that $\hbar = 1$ and $k_B = 1$. For the light-harvesting complex (a) (see Figs. 1a, 2a) all frequencies $\omega_{An1}, \ldots, \omega_{An4}$ should exceed the porphyrin transition frequency, $\omega_P = E_{P^*} - E_P$. In this case the energy of photons collected by each individual antenna can be transferred directly to the photosensitive part of the artificial reaction center (porphyrin molecule). However, in the light-harvesting complex (b) (see Figs. 1b and 2b) only the antenna An1 is coupled (by a Förster mechanism) to the porphyrin, whereas the other light-harvesting pigments form a linear chain that transfers energy downhill along the chain: An4 $\rightarrow$ An3 $\rightarrow$ An2 $\rightarrow$ An1 $\rightarrow$ P. This energy transfer can be energetically-allowed provided that $\omega_{An4} > \omega_{An3} > \omega_{An2} > \omega_{An1} > \omega_P$. In Sec. V we compare these two artificial photosystems and determine which arrangement of the antenna complexes provides more energy to the reaction center.

III. METHODS

The electron flow through a molecular triad coupled to two electron reservoirs can be described with methods of quantum transport theory and the theory of open quantum systems (see, e.g., Refs. [10, 19, 20]). In addition to four sites (D, P, P*, A), describing the molecular triad, we introduce four pairs (An1, An1*, ..., An4, An4*), which characterize the ground and excited states of the light-harvesting antennas.

The total Hamiltonian H of the system should include the two most important parts:
(i) H_0, the Hamiltonian of the electron sites and leads, including the Coulomb interaction

between the electrons located on different sites of the triad;
(ii) $H_{\rm Forster}$, which, in the case of the design in Fig. 1a, includes the direct resonant coupling between the porphyrin molecule, P, and the light-harvesting complexes An1, ..., An4.

In addition, we have to take into consideration the Hamiltonians $H_{\rm tr}$ and $H_{\rm tun}$, describing tunneling ($H_{\rm tr}$) between the electron sites on the triad and the electron reservoirs, as well as the tunneling ($H_{\rm tun}$) between the electron-binding sites belonging to the molecular triad, respectively. The interaction $H_{\rm Light}$ of the porphyrin molecule and antenna complexes with an external electromagnetic field (laser field) should also be considered because the energy dissipation due to the interaction of the antenna complex with the environment and, especially, with the blackbody radiation heat bath.

As in the experimental situation [6], we assume that a radiationless energy transfer mechanism, described by the Förster dipole-dipole matrix element (see [2, 11, 21] and references there)

$$V_{kl} = -\frac{1}{4\pi\epsilon_0\epsilon R_{kl}^3}\left[\mathbf{d}_k\cdot\mathbf{d}_l - 3\frac{(\mathbf{d}_k\cdot\mathbf{R}_{kl})(\mathbf{d}_l\cdot\mathbf{R}_{kl})}{\mathbf{R}_{kl}^2}\right], \qquad (1)$$

is mainly responsible for exciton propagation between chromophores k and l, separated by the nanoscale distance $R_{kl} = |\mathbf{R}_{kl}|$. Here ϵ_0 is the vacuum dielectric constant, and ϵ is the dielectric constant of surroundings. The matrix element V_{kl} depends on the orientations of the dipole moments $\mathbf{d}_k, \mathbf{d}_l$ of the pigments with respect to the vector $\mathbf{R}_{kl}$ between chromophores. The same mechanism provides the energy transfer between the nearest-neighbors in the antenna chain, as well as between the complex An1 and the porphyrin molecule in the linear-chain configuration shown in Fig. 1b. To estimate the value of the Förster coupling we can use a simpler formula [22]: $V_F = V_{kl} \sim d_k d_l/(2\pi\epsilon_0\epsilon R^3)$. This simplified formula is obtained assuming a parallel orientation of the respective dipole moments and coordinate vectors.

It should be emphasized that here we are interested in the steady-state regime of light-to-electricity energy conversion in the molecular triad coupled to the antenna complex. To describe this regime we use solutions of the master equations (see Appendices A and B) taken in the long-time limit. Quantum coherent effects do not play any significant role in the process since decoherence time is expected to be in the subpicosecond range even at low temperatures (see, e.g., Refs. [23–25]), whereas the time scale for the energy and charge transfer exceeds a few picoseconds [6, 15]. Our master equations are derived

when the coupling amplitudes between chromophores (V_F) and tunneling amplitudes (Δ) are smaller than the reorganization energies (describing an interaction of the system with the environment [10, 19, 20]). A standard Redfield approach [26] is able to describe quantum oscillations; however, it does not work for strong system-bath couplings.

IV. PARAMETERS

Energy levels and electrochemical potentials: The energy levels of the Fc–P–C_{60} molecular triad are $E_D = -510$ meV, $E_P = -1150$ meV, $E_{P^*} = 750$ meV and $E_A = 620$ meV. These values are obtained by estimating the reduction potentials (using a reference electrode Ag/AgCl) of ferrocene (D), porphyrin (P, P*) and fullerene (A) molecules [27]. For the electrochemical potentials of the left (μ_L) and the right (μ_R) leads, we choose the following values: $\mu_L = -410$ meV and $\mu_R = 520$ meV, with the electrochemical gradient $\Delta\mu = \mu_R - \mu_L = 930$ meV.

Coulomb interactions: The spatial separations between D–P, P–A and D–A are of order of 1.62 nm, 1.8 nm and 3.42 nm, respectively [27]. The Coulomb energies u_{DP}, u_{DA} and u_{PA} can be calculated with the formula

$$u_{ij} = \frac{e^2}{4\pi\epsilon_0\epsilon r_{ij}}$$

where, $\{ij\} = \{\mathrm{DP}\}, \{\mathrm{DA}\}, \{\mathrm{PA}\}$, e is the electron charge, and ϵ_0 is the vacuum dielectric constant. For $\epsilon \sim 4.4$, the Coulomb interaction energies are $u_{DP} = 200$ meV, $u_{DA} = 95$ meV and $u_{PA} = 180$ meV.

The Förster coupling, $V_F = V_{kl}$, between the photosensitive molecules k and l is estimated as $V_F \sim 7$ meV, if the dipole moments of the pigments satisfy $d_k \sim d_l \sim 0.1$ e·nm, and the distance $R_{kl} \sim 1$ nm.

Tunneling amplitudes: We have assumed that the ferrocene–porphyrin and porphyrin–fullerene tunneling amplitudes are about ~ 3 meV, so that

$$\frac{\Delta_{DP}}{\hbar} = \frac{\Delta_{DP^*}}{\hbar} = \frac{\Delta_{AP}}{\hbar} = \frac{\Delta_{AP^*}}{\hbar} = 4.5 \text{ ps}^{-1}.$$

For the tunneling rate Γ_L between the left lead (gold) and ferrocene, we choose the value: $\Gamma_L/\hbar = 1800$ μs^{-1}, which follows from the experimental measurements [28] of the energy-independent ferrocene-gold tunneling factor, $|T_{kL}| \sim |T_{kL}| = 6.5$ cm^{-1}, and from the formula

(B4) in the Appendix B calculated at the electron density, $\rho(\epsilon_F) \sim 0.3$ eV^{-1}atom^{-1}, for the states of gold at the Fermi energy $\epsilon_F = 5.51$ eV. For the parameter Γ_R, we use the optimal value, $\Gamma_R/\hbar = 180$ μs^{-1}, obtained in Ref. [10].

Radiation leakage and quenching rates: We take the following estimates for the radiation leakage time: $\tau_{P^*\to P} = \tau_{P^*\to D} = \tau_{A\to P} \sim 0.4$ ns. Similar estimates have been used for the radiation leakage timescales of the antenna molecules. For the quenching (or energy-loss) time of the porphyrin excited state P* we use the value: $\tau_{\rm quen} \sim 0.1$ ns.

Reorganization energies for the electron and energy transfers: For the molecular triad analyzed in Ref. [10] we obtain the relatively high power-conversion efficiency, $\eta \sim 42\%$, provided that the donor-porphyrin and acceptor-porphyrin electron transfer reorganization energies are about $\Lambda_{DP} \sim 600$ meV and $\Lambda_{AP} \sim 100 - 400$ meV. These values are close to the parameters reported in Refs. [29, 30]. A much smaller value, $\Lambda_{PP^*} \sim 100$ meV, is assumed for the light-induced electron transitions between the ground (P) and excited (P*) levels of the porphyrin molecule. The Förster energy transfer between the light-harvesting molecules and between these molecules and the porphyrin is also accompanied by an environment-reorganization process, which can be characterized by a smaller energy scale, $\Lambda_F \leq 100$ meV (see, e.g., the energy transfer in the B850 complex [31], where Λ_F is assumed to be about 30 meV).

Hereafter, we assume that the external light source has a fixed intensity, $I = 100$ mW/cm^2, and that the environment is kept at the room temperature, $T = 298$ K. We also assume that the reorganization energy for the Förster energy transfer, Λ_F, is about 100 meV, unless otherwise specified.

We analyze the Fc–P–C_{60} molecular triad, where the ferrocene molecule, Fc, is attached to the gold surface (left lead, L), and the fullerene, C_{60}, is in contact with an electrolyte solution (right lead, R) filled with oxygen molecules, which are able to accept electrons from the C_{60} molecules.

V. RESULTS AND DISCUSSION

We derive and solve numerically a set of master equations for the probabilities to find the system in a definite eigenstate of the basis Hamiltonian. This is explained in the online supplementary material. After that, we calculate: (i) the energetically-uphill electron current

through the triad, (ii) the energy of the photons absorbed by the triad and by the light-harvesting molecules. This allows us to determine a quantum yield and power-conversion efficiency of the system (see all definitions in the supporting information).

A. Photocurrent through the molecular triad directly coupled to four porphyrin light-harvesting molecules

Here we consider the situation where both the reaction center and the antenna complexes are made of porphyrin molecules with the geometrical arrangement shown in Fig. 1a. This arrangement allows direct energy transfer from each light-harvesting chromophore to the reaction center.

In Fig. 3 we plot the photocurrent through the triad as a function of the wavelength of light for different values of the Förster coupling strength : $V_F = 0, 0.1, 1, 10$ (in meV) and for the above-mentioned set of parameters of the system. It is apparent from Fig. 3 that the magnitude of the light-induced pumping current at $\lambda = 620$ nm is significantly enhanced (about 5 times larger when $V_F = 10$ meV) by the antenna system. However, the spectral range of the light absorption remains the same as for the detached porphyrin reaction center (see Fig. 3, where the red curve with square symbols describes the photocurrent through the molecular triad completely disconnected from the antenna chromophores, $V_F = 0$). We also find that the quantum yield, Φ, taken in the middle of the resonant peak ($\lambda = 620$ nm), *non-monotonically* depends on the Förster coupling strength V_F measured here in meV: $\Phi(V_F = 0) \simeq 0.85$; $\Phi(0.1) \simeq 0.3$; $\Phi(1) \simeq 0.75$ and $\Phi(10) \simeq 0.82$. It is evident from Eq. (B6), that the excitation energy transfer rate is proportional to the square, V_F^2, of the Förster coupling. Therefore, the efficiency of the excitation energy transfer processes between the antenna complexes and the reaction center should also be proportional to V_F^2 . For a sufficiently large Förster coupling, the bottleneck of the overall energy transfer process lies in the charge transfer processes. Thus, the excited states of the antenna chromophores need to wait in order to create a charge-separated state of the reaction center, due to the limited capacity of the electron transfer chain. As a result, the energy transduction efficiency does not increase linearly with the square of V_F.

B. Molecular triad connected to two BPEA and two BDPY chromophores

Now we consider a different case: an antenna system comprised of two BDPY and two BPEA molecules. The BDPY molecule has the maximum absorbance in the green region (at 513 nm) of the solar spectrum, where neither BPEA (with maximum absorbance at 450 nm) nor the porphyrin, which absorbs at 620 nm, have maxima of absorption spectra. It should be noted that a multichromophoric hexad antenna system having three light-absorbing BDPY, BPEA and porphyrin has been developed in Ref. [6], where the charge-separated state, P^{+}–C_{60}^{-}, has been generated with almost 95% quantum yield [6]. In our case, the porphyrin unit of the molecular triad is coupled to the four antenna chromophores (two BDPY and two BPEA).

We consider two situations: (a) where the antenna chromophores are *directly* coupled to the porphyrin unit of the reaction center (Fig. 1a); and (b) where the antenna chromophores are *arranged in line*: BDPY → BDPY → BPEA → BPEA → RC, with the nearest-neighbor coupling between chromophores. See Fig. 1b. Thus, the configuration (a) might appear to be energetically more efficient than (b). However, our calculations below indicate that this is not the case.

(a) For the case of direct connection between the four antennas chromophores and the triad (see Fig. 1a and Fig. 4) we calculate a photocurrent and a quantum yield, Φ, as functions of the wavelength of light, at $\Lambda_F = 100$ meV, and at five values of the Förster coupling: $V_F = 0,\ 1,\ 25,\ 50$ meV. The wavelength dependence of the current has two maxima centered at 513 nm and 620 nm. The BPEA molecules, which absorb at 450 nm, give a negligible contribution to the current since their spectral maxima are too far from the absorbance maximum of the porphyrin spectrum. As a consequence, the BPEA-porphyrin energy transfer is significantly suppressed at moderate values of the Förster reorganization energy, $\Lambda_F \leq 100$ meV in the range of the coupling constants $V_F \leq 50$ meV. It follows from Fig. 4 (see a peak at $\lambda = 513$ nm) that the BDPY molecules start working as efficient light-harvesters only at sufficiently strong Förster coupling, $V_F \geq 10$ meV, to the porphyrin unit of the molecular triad. We also note that when $\lambda \sim 513$ nm, both the photoinduced current and the quantum yield grow with increasing the Förster coupling strength, so that the quantum yield, Φ, can be around 48%. In the range of porphyrin absorption (at $\lambda \sim 620$ nm and $V_F = 0$) the quantum yield is of the order of 90%.

(b) A much broader light spectrum can be converted into electrical current in the linear configuration in Fig. 1b, where the light-harvesting chromophores are arranged along a line: BPEA $\rightarrow$ BPEA $\rightarrow$ BDPY $\rightarrow$ BDPY $\rightarrow$ RC, with the only one BDPY molecule directly coupled to the porphyrin unit of our artificial reaction center (RC) (see Fig. 1b and Fig. 5). This system is able to collect photons in the range of wavelength from 420 nm up to 650 nm covering a significant part of the visible sunlight spectrum. The chain of BPEA and BDPY molecules creates an efficient channel, which gradually transmits energy from the collectors of high-energy photons (BPEA molecules), via the intermediate BDPY antennas, to the molecular triad. In Figs. 5a, 5b we plot the photoinduced current and the quantum yield versus the wavelength of the external radiation, at $\Lambda_F = 100$ meV, and at four values of the Förster constants (in meV) $V_F = 0,\ 1,\ 25,\ 50$. For large value of the Förster coupling strength V_F the quantum yield Φ reaches $\sim 48\%$ in Fig.4(a) around $\lambda = 513$ nm [for the star-shaped topology in Fig. 1a] and $\sim 30\%$ in Fig. 5(b) [for the linear chain case in Fig 1b]. The quantum yield in Fig. 5b is lower than the one in Fig. 4a, but extends over a wider range of wavelengths including the peaks around $\lambda \sim 450$ nm and $\lambda \sim 513$ nm.

It follows from Fig. 4 and Fig. 5, that the configuration using the chain-like nearest-neighbor coupling between light-harvesting chromophores [Fig. 1b, design (b)] converts much more blue ($\lambda = 450$ nm) light into electricity with a higher quantum yield than the star-shaped configuration with direct coupling between the antenna chromophores and the RC [Fig. 1a, design (a)]. In this star-shaped configuration, the BPEA molecules, which collects blue photons, are *not* able to transfer their energy to the photosensitive unit of the triad due to a significant difference between the energies of the BPEA antennas ($\lambda = 450$ nm) and the porphyrin-based reaction center ($\lambda = 620$ nm).

The antenna-RC energy transfer is facilitated by the strong coupling to the environment (when the energy difference is high), characterized by the reorganization energy Λ_F, as well as by a tight Förster binding between chromophores, which is described by the constant V_F. In Figs. 6 and 7 we plot the quantum yield, Φ, as a function of the reorganization energy, Λ_F, for three different temperatures (in K): $T = 77$, 298, 500, and for three values of the coupling constant $V_F = 1,\ 25,$ and 50 meV. Figure 6 is related to the blue peak of the absorption spectrum ($\lambda = 450$ nm), whereas figures 7 describes the behavior of the green peak ($\lambda = 513$ nm). The peak centered at $\lambda = 620$ nm is produced by the porphyrin molecule, belonging to the triad, and, therefore, shows no dependence on Λ_F and V_F.

The Marcus rates, describing the energy transmission between the photosensitive elements of the system, depend (i) on the energy difference, ΔE, between the photosensitive units, (ii) on the Förster coupling V_F, and (iii) on the Förster reorganization energy Λ_F. The large energy separation, ΔE, of the energies of the nearby photosensitive molecules leads to a decrease of the Marcus rates and, thus, to the suppression of the energy transfer. In our case, the energy distance between the BPEA ($\lambda = 450$ nm) and BDPY ($\lambda = 513$ nm) molecules is about 340 meV, whereas the energy separation of the BDPY chromophore and porphyrin ($\lambda = 620$ nm) is of order of 415 meV. This energy gap can be partially compensated by the large reorganization energy, Λ_F, which reflects the significant fluctuations of the relative positions of the energy levels. Here, the environment plays a positive role assisting the efficient and fast energy transfer between chromophores (see also Ref. [11, 13, 26]). The timescales for the energy and electron transfers should be shorter than the radiation leakage time and the quenching time, otherwise the energy of the photons absorbed by the system will be lost.

At low temperatures (e.g., liquid nitrogen, $T = 77$ K), the fluctuations in the positions of the energy levels of the chromophores are frozen, so that the light-to-electricity conversion requires sufficiently large values of the reorganization energy, $\Lambda_F > 180$ meV (see Figs. 6a and 7a). Note that for $V_F > 25$ meV the linear-chain arrangement system has an optimal performance at $\Lambda_F \simeq 225$ meV for both frequency ranges. This extreme low temperature case is only shown for comparison with the higher temperatures cases.

At room temperature ($T = 298$ K) and at strong enough Förster coupling, $V_F \geq 25$ meV, the blue and green spectral peaks demonstrate similar behaviors as functions of Λ_F (see Figs. 6b and 7b). Here, the quantum yield begins to grow when the reorganization energy exceeds ~ 80 meV, reaching finally 90% at $\Lambda_F > 150$ meV. These numbers are determined by the parameters of the antenna-triad complex, and, especially, by the radiation leakage time $\tau_{\rm rad}$, of the excited porphyrin state P*, estimated above as $\tau_{\rm rad} \sim 0.4$ ns.

At high temperatures (see Figs. 6c and 7c, plotted for $T = 500$ K) the facilitating effect of the environment increases, and the efficient energy transfer starts at the lower reorganization energies, $\Lambda_F \geq 75$ meV. This value of Λ_F is comparable with the reorganization energy for the energy transfer in the B850 light-harvesting complex, where $\Lambda_F \simeq 27$ meV [31].

At the smaller value of the Förster coupling, $V_F = 1$ meV, the conversion of the blue light ($\lambda = 450$ nm) to electricity is significantly suppressed (see Fig. 6), whereas for green light ($\lambda = 513$ nm) the dependence of the quantum yield on Λ_F are shifted to higher reorganization

energies (Fig. 7), compared to the case of the larger couplings, $V_F = 25,\ 50$ meV.

It should be noted that, to cover a broader range of the spectrum of light with a fixed number of antenna chromophores, the resonance energies of the light-harvesting complexes should be very well separated. However, in this case the energy transfer between the antenna chromophores would be quite slow, since this transfer is governed by the rates corresponding to the inverted regions of the Marcus parabola [32]. Then, the dissipation comes into play, and the energy of the absorbed photons is lost on its way from the antennas to the reaction center. The energy transfer rates and, thus, the efficiency of the system can be maximized in the case when the energy distance, $\Delta E_i = E_{i+1} - E_i$, between the nearby light-harvesting complexes (labeled by indices $i+1$ and i, with energies E_{i+1} and E_i) is equal to the corresponding reorganization energy, Λ_F^i. That is, $\Delta E_i = E_{i+1} - E_i = \Lambda_F^i$. We note that for a system with identical antennas, the star-like configuration provides more energy to the reaction center than the linear one, although the latter one covers a narrower range of sunlight spectrum.

VI. CONCLUSIONS

In this paper we have studied theoretical aspects of the operation of an artificial reaction center (a ferrocene–porphyrin–fullerene molecular triad) coupled to the complex of four light-harvesting molecules. We have analyzed two configurations of the antenna complex: (a) a star-shaped configuration, where each light-harvesting molecule is able to transfer energy directly to the centrally-located reaction center, and (b) a case where the antenna molecules form a linear chain, which gradually transfers excitations from the high-energy antenna located in the far end, to the antenna chromophore with the lowest energy. The last antenna chromophore in the chain is energetically connected to the reaction center (RC). To be specific, we have considered the case when the antenna complex is comprised of two molecules of bis(phenylethynyl)anthracene (BPEA), absorbing blue photons ($\lambda = 450$ nm), and two molecules of borondipyrromethene (BDPY), having an absorption maximum in the green region ($\lambda = 513$ nm). We have shown that the configuration with a linear arrangement of the antenna chromophores (configuration (b)) is able to convert blue and green photons to electricity with a quantum yield of order of $\sim$30% (over a wide range of wavelengths), whereas the energy of the red photons, absorbed by the molecular triad itself

($\lambda = 620$ nm), is converted to a current with a quantum yield reaching the value of 90%. We have investigated dependencies of the quantum yield on the Förster reorganization energy as well as on the Förster coupling constants between chromophores and have shown that the environment plays a significant role in facilitating the antenna-RC energy transfer, thus, improving the light-harvesting function of the system. Overall, the configuration (b) is more efficient than (a) in transferring energy to the reaction center. A similar conclusion takes place for the case of many antenna pigments coupled to the artificial reaction center.

We emphasize that the artificial photosystem analyzed in this work can be implemented with real light-harvesting components, such as porphyrin and BPEA/BDPY molecules. The excitonic (Förster) coupling strongly depends on the mutual distances and the orientations of the chromophores. Similar to the wheel-shaped antenna-reaction center complex implemented in Ref. [6], the components of the photosystem can be placed at distances of the order 10 Å, which allows for a sufficiently strong Förster coupling between the antenna chromophores and the reaction center. At the same time, the chromophores comprising the light-harvesting complex retain their individual molecular features. The reorganization energy, another controlling parameter for energy transfer, is varied for the system under study. Namely, we numerically calculate both the light-induced electron current and the quantum yield as functions of the reorganization energy. This allows us to determine the value of the reorganization energy at which the system works with maximum optimal efficiency.

Acknowledgements. We thank the RIKEN RICC for providing computing resources. PKG is supported by JSPS Foreign Postdoctoral Fellowship No. P11502. FN acknowledges partial support from the Laboratory of Physical Sciences, National Security Agency, Army Research Office, DARPA, National Science Foundation grant No. 0726909, JSPS-RFBR contract No. 09-02-92114, Grant-in-Aid for Scientific Research (S), MEXT Kakenhi on Quantum Cybernetics, and Funding Program for Innovative Research and Development on Science and Technology (FIRST).

Appendix A: Hamiltonian

Here we describe the methods used in our work. We characterize the electrons in the states i (= D, P, P*, An1, An1*, An2, An2*, An3, An3*, An4, An4*, A) by the Fermi operators a_i^+ and a_i with the electron population operator $n_i = a_i^+ a_i$. Each electron state

can be occupied by a single electron, as the spin degrees of freedom are neglected. Electrons in the leads (electrodes) are described by the Fermi operators $d^+_{k\alpha}, d_{k,\alpha}$, where $\alpha = \mathrm{L}, \mathrm{R}$; and k is an additional parameter which has the meaning of a wave vector in condensed matter physics. The number of electrons in the leads is determined by the operator $\sum_k N_{k\alpha}$, with $N_{k\alpha} = d^+_{k\alpha} d_{k\alpha}$. The total Hamiltonian of the system is complicated. It includes the terms described below.

1. Eigenenergies and Coulomb interactions

This part of the Hamiltonian involved the eigenenergies of the electron states (i = D, P, P*, An1, An1*, An2, An2*, An3, An3*, An4, An4*, A) and the Coulomb interactions between the electron states.

$$\begin{aligned} H_0 \;=\; & \sum_i E_i n_i + u_P n_P n_{P^*} + u_{DP}(1-n_D)(1-n_P-n_{P^*}) \\ - \; & u_{DA}(1-n_D)n_A - u_{PA}(1-n_P-n_{P*})n_A. \end{aligned} \tag{A1}$$

The symbols $u_P, u_{DP}, u_{DA}, u_{PA}$ represent the electrostatic interactions between the electron sites. We have assumed that the empty donor state D (with $n_D = 0$) as well as the empty photosensitive group ($n_P + n_{P^*} = 0$) have positive charges. Therefore, $U_{DP} > 0$ because both D and P are positively charged and thus repulsive. The acceptor state A becomes negatively charged when it is occupied by an electron and thus $-U_{DA} < 0$ and $-U_{PA} < 0$. This attraction occurs when the acceptor A is occupied ($n_A = 1$) and the D and P states are both empty. Also, the acceptor state A is neutral when it is empty. The antenna pigments, An1 - An4, are coupled to each other and to the reaction center via dipole-dipole resonant coupling. They exchange only excitation energies but not electrons. Therefore, they always remain uncharged, so that there are no Coulomb interactions between the antennas and other components of the photosystem.

2. Förster couplings

We consider the energy transfer between the reaction center (P) and the antenna complexes, and also among the antenna complexes by introducing Förster coupling terms,

$$H_{\text{Forster}} = -\sum_{kl} V_{kl}\, a_l^+\, a_{l^*}\, a_{k^*}^+\, a_k + \text{H.c.}\,, \tag{A2}$$

where the pair $\{k, l\} = \{\text{P, An1}\}$, $\{\text{P, An2}\}$, $\{\text{P, An3}\}$, $\{\text{P, An4}\}$, $\{\text{An1, An2}\}$, $\{\text{An2, An3}\}$, $\{\text{An3, An4}\}$. Here, V_{kl} (1) determines the strength of the Förster coupling. We use notation V_F instead of V_{kl} in the text.

3. Tunneling couplings to the leads

The electron tunnelling from the left lead to the donor state and from the acceptor state to the right lead are both given by the Hamiltonian,

$$H_{\text{tr}} = -\sum_k T_{kL}\, a_D^+\, c_{kL} - \sum_k T_{kR}\, c_{kR}^+\, a_A + \text{H.c.}\,, \tag{A3}$$

where $c_{k\alpha}^+, c_{k\alpha}$ are the electron creation and annihilation operators, and α is the index for the leads. The Hamiltonian of the leads is given by

$$H_{LR} = \sum_\alpha \varepsilon_\alpha n_\alpha \qquad \text{with} \qquad n_\alpha = \sum_k c_{k\alpha}^+\, c_{k\alpha}\,.$$

4. Electron tunneling

Tunneling of electrons between components of the molecular triad is described by the Hamiltonian H_{tun},

$$H_{\text{tun}} = -\sum_l \Delta_{l,l'}\, a_l^+\, a_{l'} + \text{H.c.}\,, \tag{A4}$$

Here $\Delta_{l,l'}$ is the strength of the tunnelling coupling and the $\{l, l'\}$ indices refer to the pairs: $\{\text{D, P}\}$, $\{\text{D, P}^*\}$, $\{\text{A, P}\}$, $\{\text{A, P}^*\}$.

5. Light-induced excitations

This part of the Hamiltonian accounts for the interaction of light with the molecular triad and the antenna complexes. Under the rotating-wave approximation, the light-induced

excitation processes can be described as

$$H_{\text{Light}} \;=\; -\;\sum_{k} F\, e^{i\omega_0 t}\, a_k^{+}\, a_{k^*} \;+\; \text{H.c.} \tag{A5}$$

where k = P, An1, An2, An3, An4 and the field amplitude

$$F = \mathcal{E}_{\text{ext}}\; d_{kk^*}\;,$$

where d_{kk^*} is the dipole moment of the $k-$chromophore.

6. Coupling to a radiation heat bath and an Ohmic bath

Coupling the system to a radiation heat bath causes radiation leakage from the excited states. The following Hamiltonian accounts for this radiation leakage

$$H_Q = -\sum_{\sigma} Q_{\sigma\sigma'} a_\sigma^{+} a_{\sigma'} + \text{H.c.}\;, \tag{A6}$$

where $\{\sigma, \sigma'\}$ denotes the pairs of sites {D, P*}, {A, P}, {P, P*}, {An1,An1*}, {An2, An2*}, {An3, An3*}, {An4, An4*}.

The operators for the radiation bath,

$$Q_{\sigma\sigma'} = e\; x_{\sigma\sigma'} \times \mathcal{E}_{\text{rad}} \tag{A7}$$

are proportional to the projection of the fluctuating electromagnetic field, $\mathcal{E}_{\text{rad}}$, along the direction of the corresponding dipole moment, $d_{\sigma\sigma'} = e\, x_{\sigma\sigma'}$. The fluctuations of the blackbody radiation field are assumed to be isotropic.

The excited state of the photosensitive part of the molecular triad can be quenched by the electrode. Namely, lose the excitation energy when interacting with the electrodes. We introduce H_{quench} to account for this energy-loss or quenching processes.,

$$H_{\text{quench}} = -Q_l\, a_l^{+}\, a_{l'} + \text{H.c.}\;, \tag{A8}$$

where, Q_l is the variable of the Ohmic bath and $\{l, l'\}$ = {P, P*}.

7. Interaction with the environment

We have taken into account the effects of a dissipative environment by the well-known system-reservoir model [19, 32]:

$$H_{\text{env}} = \;\sum_{j}\left[\frac{p_j^2}{2m_j} + \frac{m_j\omega_j^2}{2}\left(x_j + \frac{1}{2}\sum_i x_{ji}\; n_i\right)^2\right],$$

(A9)

where x_j, p_j are the position and momentum of the jth oscillator with effective masses m_j and frequencies ω_j, and n_i are populations of electron sites in the system including ground and excited states of antenna pigments. Here, x_{ji} is a measure of the strength of the coupling between the electron subsystem and the environment. We characterize the phonon modes of the bath by the spectral functions $J_{ii'}(\omega)$, defined by

$$J_{ii'}(\omega) = \sum_j \frac{m_j \omega_j^3 (x_{ji} - x_{ji'})^2}{2} \delta(\omega - \omega_j) \ . \tag{A10}$$

The spectral function $J_{ii'}$ is related to the reorganization energy $\Lambda_{ii'}$ for the $i \to i'$ transition, by the following equation:

$$\Lambda_{ii'} = \int_0^\infty \frac{d\omega}{\omega} J_{ii'}(\omega) = \sum_j \frac{m_j \omega_j^2 (x_{ji} - x_{ji'})^2}{2}. \tag{A11}$$

Appendix B: Master equations

The system under study can be characterized by the 256 eigenstates of H_0. We expressed all the operators described in previous section in terms of the density operators $\rho_{\mu\nu} \equiv |\mu\rangle\langle\nu|$. To derive the time evolution of the diagonal elements $\rho_{\mu\mu} \equiv \rho_\mu$ of the density matrix $(\rho_{\mu\nu})$, we write the Heisenberg equation for the operators, with the subsequent averaging $\langle\rho_\mu\rangle$ over the environment fluctuations. Assuming (see, e.g., [19, 20]) that the transition amplitudes (dipole-dipole elements V_F and electron tunneling rates Δ) of the photosystem are much less than the reorganization energies Λ, and for the case of environment with sufficiently high temperature we obtain the master equations for the density matrix of the system [10, 20],

$$\langle\dot{\rho}_\mu\rangle + \sum_\nu \gamma_{\nu\mu}\langle\rho_\mu\rangle = \sum_\nu \gamma_{\mu\nu}\langle\rho_\nu\rangle, \tag{B1}$$

where $\gamma_{\mu\nu}$ is the total relaxation matrix, which is the sum of six types of relaxation rates:

$$\gamma_{\mu\nu} = \gamma_{\mu\nu}^{\rm tr} + k_{\mu\nu}^{\rm Forster} + k_{\mu\nu}^{\rm tun} + k_{\mu\nu}^{\rm light} + k_{\mu\nu}^{\rm rad} + k_{\mu\nu}^{\rm quench} \ . \tag{B2}$$

These relaxation rates will be described right below.

1. Electron tunneling rates between the leads and the molecular triad

The first term of Eq.(B2), $\gamma^{\rm tr}_{\mu\nu}$, represents the relaxation rates due the couplings of the triad to the L and R electron reservoirs:

$$\begin{aligned}\gamma^{\rm tr}_{\mu\nu} = \Gamma_L \left\{|a_{D;\mu\nu}|^2[1-f_L(\omega_{\nu\mu})] + |a_{D;\nu\mu}|^2 f_L(\omega_{\mu\nu})\right\} \\ +\Gamma_R \left\{|a_{A;\mu\nu}|^2[1-f_R(\omega_{\nu\mu})] + |a_{A;\nu\mu}|^2 f_R(\omega_{\mu\nu})\right\} \ , \end{aligned} \tag{B3}$$

where, the the resonant tunneling rates, Γ_α ($\alpha = {\rm L}, {\rm R}$), are related to the energy independent tunneling factor by the following equation,

$$\Gamma_{L\alpha} = 2\pi \sum_k |T_{k\alpha}|^2 \delta(\omega - \epsilon_{k\alpha}) \tag{B4}$$

$|T_{k\alpha}|$ is the energy-independent tunneling factor.

Here, the electron reservoirs have been characterized by the Fermi distributions $f_\alpha(\omega)$,

$$f_\alpha(E_{k\alpha}) = \left[\exp\left(\frac{E_{k_B\alpha} - \mu_\alpha}{T}\right) + 1\right]^{-1} . \tag{B5}$$

with the temperature T ($k_{\rm B} = 1, \hbar = 1$). The electrochemical potentials μ_L and μ_R are the controlling factors of the electron transition rates from the left lead to the donor state, and from the acceptor state to the right lead.

2. Förster relaxation rates

Here $k^{\rm Forster}_{\mu\nu}$ accounts for the excitation transfer rates from the antenna complexes to the reaction center, and also among the antenna complexes. The excitation transition rates via the Förster mechanism can be derived with the methods described in Refs.[9, 10, 20]

$$\begin{aligned}\kappa^{\rm Forster}_{\mu\nu} \ &= \ \sum_{kl} \sqrt{\frac{\pi}{\Lambda_{kl} T}} \ |V_{kl}|^2 \ \left[|(a_l^+ a_{l^*} a^+_{k^*} a_k)_{\mu\nu}|^2 \right. \\ &+ \ \left. |(a_l^+ a_{l^*} a^+_{k^*} a_k)_{\nu\mu}|^2\right] \exp\left[-\frac{(\omega_{\mu\nu} + \Lambda_{kl})^2}{4\Lambda_{kl} T}\right] \ , \end{aligned} \tag{B6}$$

where V_{kl} is the resonant Förster relaxation rate and Λ_{kl} stands for reorganization energy. We denote, $V_{kl} = V_F$ and $\Lambda_{kl} = \Lambda_F$ for any combinations of k and l. The non-resonant exponential term of the above expression arises due to the different energy gaps of the reaction center and the accessory antenna complexes. Moreover, the non-resonant exponential terms depend on the reorganization energy.

3. Thermal tunneling rates

The matrix element $k_{\mu\nu}^{\rm tun}$ of the Eq. (B2) are responsible for the relaxation processes arising from thermal tunneling. These are given by

$$\begin{aligned}\kappa_{\mu\nu}^{\rm tun} &= \sum_{\sigma\sigma'}\sqrt{\frac{\pi}{\Lambda_{\sigma\sigma'}T}}\ |\Delta_{\sigma\sigma'}|^2\ \left[|(a_\sigma^+ a_{\sigma'})_{\mu\nu}|^2\right. \\ &+\ \left.|(a_\sigma^+ a_{\sigma'})_{\nu\mu}|^2\right]\exp\left[-\frac{(\omega_{\mu\nu}+\Lambda_{\sigma\sigma'})^2}{4\Lambda_{\sigma\sigma'}T}\right]\ ,\end{aligned} \tag{B7}$$

where Δ is the resonant tunnelling rate, $\omega_{\mu\nu}$ is the energy difference between the states μ and ν (acting as a thermodynamic gradient), and the reorganization energy Λ are the main guiding factors of the thermal tunneling rates $\kappa_{\mu\nu}^{\rm tun}$. Details of derivation can be found in Ref. [10, 20].

4. Light-induced excitation rates

As in Ref. [10] the contribution $k_{\mu\nu}^{\rm light}$ to the total relaxation matrix due to light-induced excitation processes is

$$\begin{aligned}\kappa_{\mu\nu}^{\rm light} &= \sum_k |F|^2\sqrt{\frac{\pi}{\Lambda_{\sigma\sigma^*}T}}\left\{|(a_\sigma^+ a_{\sigma^*})_{\mu\nu}|^2\right. \\ &\times\ \exp\left[-\frac{(\omega_{\mu\nu}+\omega_0+\Lambda_{\sigma\sigma^*})^2}{4\Lambda_{\sigma\sigma^*}T}\right] \\ &+\ \left.|(a_\sigma^+ a_{\sigma^*})_{\nu\mu}|^2\exp\left[-\frac{(\omega_{\mu\nu}-\omega_0+\Lambda_{\sigma\sigma^*})^2}{4\Lambda_{\sigma\sigma^*}T}\right]\right\}\end{aligned} \tag{B8}$$

This rate includes contributions from the following transitions, P$\rightarrow$P*, An1 $\rightarrow$ An1*, An2 $\rightarrow$ An2*, An3 $\rightarrow$ An3*, and An4 $\rightarrow$ An4*.

5. Relaxation rates due to radiation leakage

Neglecting the effects of the environment on the radiation transitions, $k_{\mu\nu}^{\rm rad}$ is given by

$$\begin{aligned}\kappa_{\mu\nu}^{\rm rad} &= \frac{2n}{3}\sum_{\sigma\sigma'}|d_{\sigma\sigma'}|^2\ [|(a_\sigma^+ a_{\sigma'})_{\mu\nu}|^2+|(a_\sigma^+ a_{\sigma'})_{\nu\mu}|^2] \\ &\times\ \left(\frac{\omega_{\mu\nu}}{c}\right)^3\left[\coth\left(\frac{\omega_{\mu\nu}}{2T}\right)-1\right]\ ,\end{aligned} \tag{B9}$$

where n and $d_{\sigma\sigma'}$ stand for the refraction index and the dipole moment, respectively [10].

6. Lead-induced quenching rates of the excited states

The last term of Eq. (B2), $k_{\mu\nu}^{\rm quench}$, describes the energy loss due to the quenching of the excited state of the photosensitive part of the triad.

$$\begin{aligned}\kappa_{\mu\nu}^{\rm quench} &= \alpha_p[|(a_P^+ a_{P^*})_{\mu\nu}|^2 + |(a_P^+ a_{P^*})_{\nu\mu}|^2] \\ &\times \omega_{\mu\nu}\left[\coth\left(\frac{\omega_{\mu\nu}}{2T}\right) - 1\right] . \end{aligned} \tag{B10}$$

Appendix C: Current and efficiency

1. Electron current

For weak couplings, the electron flowing (particle current) between the leads and the molecular triad is given by:

$$I_e = I_R = \left(\frac{d}{dt}\right)\sum_k \langle c_{kR}^+ c_{kR}\rangle ,$$

We derive the equation of the current in terms of the density matrix elements,

$$\begin{aligned} I_e &= \Gamma_R \sum_{\mu\nu} |a_{A;\mu\nu}|^2 [1 - f_R(\omega_{\nu\mu})]\langle\rho_\nu\rangle \\ &- \Gamma_R \sum_{\mu\nu} |a_{A;\mu\nu}|^2 f_R(\omega_{\nu\mu})\langle\rho_\mu\rangle . \end{aligned} \tag{C1}$$

2. Absorbed energy

The total amount of energy absorbed per unit time $\mathcal{E}_{\rm photon}$ by the molecular triad and antenna chromophores is

$$\begin{aligned}\mathcal{E}_{\rm photon} &= \sum_\sigma \omega_0 |F|^2 \sqrt{\frac{\pi}{\Lambda_{\sigma\sigma^*} T}} \sum_{\mu\nu} |(a_\sigma^+ a_\sigma)_{\mu\nu}|^2 \langle\rho_\mu - \rho_\nu\rangle \\ &\times \left(\exp\left[-\frac{(\omega_{\mu\nu} - \Lambda_{\sigma\sigma^*} + \omega_0)^2}{4\Lambda_{\sigma\sigma^*} T}\right]\right. \\ &- \left.\exp\left[-\frac{(\omega_{\mu\nu} - \Lambda_{\sigma\sigma^*} - \omega_0)^2}{4\Lambda_{\sigma\sigma^*} T}\right]\right) , \end{aligned} \tag{C2}$$

where σ = P, An1, An2, An3, An4.

3. Power-conversion efficiency

The power-conversion efficiency of the system is the ratio of the output $E_{\rm output}$ and the input $E_{\rm input}$ energies,

$$\eta = \frac{E_{\rm output}}{E_{\rm input}} = \frac{\mathcal{E}_{\rm pump}}{\mathcal{E}_{\rm photon}} = \frac{I_R(\mu_R - \mu_L)}{\mathcal{E}_{\rm photon}}. \tag{C3}$$

The quantum yield is defined as

$$\Phi = \frac{n_{\rm pump}}{N_{\rm photon}} = \eta \, \frac{\hbar\omega_0}{\mu_R - \mu_L} \, . \tag{C4}$$

---

[1] R. E. Blankenship 2002 *Molecular mechanisms of photosynthesis* (Oxford: Blackwell Science).

[2] H. V. Amerongen, L. Valkunas and R. Van Grondelle 2000 *Photosynthetic Excitons* (Singapore: World Scientific).

[3] D. Kuciauskas, P. A. Liddell, S. Lin, T. E. Johnson, S. J. Weghorn, J. S. Lindsey, A. L. Moore, T. A. Moore and D. Gust, J. Am. Chem. Soc. **121**, 8604 (1999).

[4] H. Imahori, J. Phys. Chem. B **108**, 6130 (2004).

[5] H. Imahori, Bull. Chem. Soc. Jpn. **80**, 621 (2007).

[6] G. Kodis, Y. Terazono, P. A. Liddell, J. Andréasson, V. Garg, M. Hambourger, T. A. Moore, A. L. Moore and D. Gust, J. Am. Chem. Soc. **128**, 1818 (2006).

[7] D. Gust, T. A. Moore and A. L. Moore, Acc. Chem. Res. **42**, 1890 (2009).

[8] A. M. Ferreira and D. Bashford, J. Am. Chem. Soc. **128**, 16778 (2006).

[9] P. K. Ghosh, A. Yu. Smirnov and F. Nori, J. Chem. Phys. **131**, 035102 (2009).

[10] A. Yu. Smirnov, L. G. Mourokh, P. K. Ghosh and F. Nori, J. Phys. Chem. C **113**, 21218 (2009); P. K. Ghosh, A. Yu. Smirnov and F. Nori, J. Chem. Phys. **134**, 244103 (2011).

[11] M. Mohseni, P. Rebentrost, S. Lloyd and A. Aspuru-Guzik, J. Chem. Phys. **129**, 174106 (2008).

[12] M. B. Plenio and S. F. Huelga, New J. Phys. **10**, 113019 (2008).

[13] P. Rebentrost, M. Mohseni, I. Kassal, S. Lloyd and A. Aspuru-Guzik, New J. Phys. **11**, 033003 (2009).

[14] F. Caruso, A. W. Chin, A. Datta, S. F. Huelga and M. B. Plenio, J. Chem. Phys. **131**, 105106 (2009).

[15] Y. Terazono, G. Kodis, P. A. Liddell, V. Garg, T. A. Moore, A. L. Moore and D. Gust, J. Phys. Chem. B. **113**, 7147 (2009).

[16] Y. Terazono, G. Kodis, K. Bhushan, J. Zaks, C. Madden, A.L. Moore, T.A. Moore, G.R. Fleming, D. Gust, J. Am. Chem. Soc. **133**, 2916 (2011).

[17] D. Gust, A. T. Moore and A. L. Moore, Acc. Chem. Res. **811**, 265 (1985).

[18] R. W. Wagner and J. S. Lindsey, J. Am. Chem. Soc. **116**, 9759 (1994).

[19] D. A. Cherepanov, L. I. Krishtalik and A. Y. Mulkidjanian, Biophys. J. **80**, 1033 (2001).

[20] A. Yu. Smirnov, L. G. Mourokh and F. Nori, J. Chem. Phys. **130**, 235105 (2009).

[21] P. Rebentrost, M. Stopa M and A. Aspuru-Guzik, Nanoletters **10**, 2849 (2010).

[22] A. Yu. Smirnov, L. G. Mourokh and F. Nori, Phys. Rev. E **77**, 011919 (2008).

[23] E. Collini and G. D. Scholes, Science **323**, 369 (2009).

[24] G. Panitchayangkoon, D. Hayes, K. A. Fransted, J. R. Caram, E. Harel, J. Wen, R. E. Blankenship and G. S. Engel, Proc. Natl. Acad. Sci. U.S.A. **107**, 12766 (2010).

[25] Y-C. Cheng and G. R. Fleming, Annu. Rev. Phys. Chem. **60**, 241 (2009).

[26] M. Yang and G. R. Fleming, Chem. Phys. **282**, 163 (2002).

[27] H. Imahori, H. Yamada, Y. Nishimura, I. Yamazaki, and Y. Sakata, J. Phys. Chem. B **104**, 2099 (2000).

[28] K. Weber, L. Hockett and S. Creager, J. Phys. Chem. B **101**, 8286 (1997).

[29] H. Imahori, H. Yamada, D. M. Guldi, Y. Endo, A. Shimomura, S. Kundu, K. Yamada, T Okada, Y. Sakata and S. A. Fukuzumi, Engew. Chem., Int. Ed. **41**, 2344 (2002).

[30] H. Imahori, N. V. Tkachenko, V. Vehmanen, K. Tamaki, H. Lemmetyinen, Y. Sakata and S. Fukuzumi, J. Phys. Chem. A **105**, 1750 (2001).

[31] V. Urboniene, O. Vrublevskaja ,G. Trinkunas , A. Gall, B. Robert and L. Valkunas, Biophys. J. **93**, 2188 (2007)

[32] R. A. Marcus and N. Sutin, Biochim. Biophys. Acta. **811**, 265 (1985).

Figure captions

FIG.1: (Color online) Schematic diagram of an artificial photosystem comprised of a molecular triad (D–P–A) and four additional light-harvesting complexes (An1, An2, An3, An4). Here, D = donor, A = acceptor, and P = photosensitive part (porphyrin). The molecular triad D–P–A is inserted between two electrodes (leads) L and R. Energy exchange processes are denoted by straight red arrows. The green bent curved arrows describe electron pathways, L $\rightarrow$ D $\rightarrow$ P $\rightarrow$ A $\rightarrow$ R, via the molecular triad. (a) The photosensitive part, P, of the molecular triad is surrounded by four accessory light-harvesting complexes An1, An2, An3, and An4. In this case the surrounding antenna complexes can transfer excitations to the reaction center directly. (b) Here the antenna complexes form a linear chain coupled to the reaction center via nearest-neighbor couplings.

FIG.2: (Color online) Energy diagram of the antenna complexes An1, ..., An4, energetically coupled to the reaction center (RC), D–P–A, for the case (a) where each light-harvesting molecule is directly connected to the porphyrin molecule, P, of the RC; and (b) where the energy transfer occurs via a linear-chain of antenna with nearest-neighbor energy exchange. Note that the four antenna chromophores in (b) are arranged in a way to have a relatively small energy difference between neighboring units.

FIG.3: (Color online) Photoinduced electron current I_e (number of electrons, in one ms, pumped from the L to the R lead) versus the wavelength of the incident light for a photosystem with four antenna complexes, which are made of porphyrin molecules. Both the antenna complexes and the reaction center absorb at the same wavelength. The whole complex now absorbs more photons than the single porphyrin molecule; thus, pumping many more electrons from the left (with $\mu_L = -410$ meV) to the right (with $\mu_R = 520$ meV) electron reservoir. The other parameters are listed in the text (see Sec. IV). The peak in the current increases for larger values of the Förster coupling strength V_F. We also studied (not shown here) higher values of V_F, but these produced the same results as $V_F = 10$ meV. Thus, this value of V_F provides a saturation in the electron current. The resonant peak here is $\lambda = 620$ nm. It follows from Eq. (B8), that the light-induced excitation rate of porphyrin, P, is maximized when $\omega_0 = \Delta E_{PP*} + \Lambda_{PP*} \sim$ 2000 meV, which corresponds to the resonance peak around 620 nm.

FIG.4: (Color online) Electron current I_e and quantum yield Φ as functions of the wavelength λ of the external radiation for the configuration shown in Fig. 1a, where two BPEA and two

BDPY antenna chromophores are directly coupled to the centrally-located reaction center. The Förster coupling constant, V_F, which is assumed to be the same for every chromophore-RC connection, takes four values (in meV): $V_F = 0,\ 1,\ 25,\ 50$. For other parameters see Sec. IV. Note that the electron current and the quantum yield grow for increasing values of the Förster coupling energy strength V_F. More importantly, the direct coupling (Fig. 1a) suppresses the peak at λ= 450 nm (Fig. 4a), which is present in the linear chain configuration (Fig. 1b), as shown in Fig. 5a.

FIG.5: (Color online) Electron current I_e and a quantum yield Φ versus the wavelength of light, λ, for the configuration shown in Fig. 1b, where the excitation energy moves along the following chain of light-harvesting molecules: BPEA $\rightarrow$ BPEA $\rightarrow$ BDPY $\rightarrow$ BDPY $\rightarrow$ RC. The parameters used here are the same as in Fig. 4. However, the current peak at $\lambda \sim 450$ nm is present in (a) here, but absent in Fig. 4(a), which used a direct-coupling configuration to the central reaction center.

FIG.6: (Color online) Quantum yield as a function of reorganization energy, Λ_F, for the linear-chain nearest-neighbor coupling between chromophores, BPEA $\rightarrow$ BPEA $\rightarrow$ BDPY $\rightarrow$ BDPY $\rightarrow$ RC, for a the wavelength of light $\lambda = 450$ nm (blue peak in Fig. 5a). This figure is plotted for three different temperatures: (a) Low $T = 77$ K, (b) room temperature $T = 298$ K and (c) very high $T = 500$ K as well as for three values of the Förster constant $V_F = 1,\ 25$, and 50 meV. As shown in the figures (b) and (c), increasing the reorganization energy Λ_F, can sharply increase the quantum yield. The extreme low-temperature case in (a) is just a limit case, shown for comparison with the higher-temperature cases in (b) and (c).

FIG.7: (Color online) Quantum yield versus reorganization energy, Λ_F, for the green peak ($\lambda = 513$ nm) of the spectrum (see Fig. 5a) for three values of the Förster constant, $V_F = 1,\ 25,\ 50$ meV, and at three different temperatures: (a) $T = 77$ K, (b) $T = 298$ K and (c) $T = 500$ K. The other parameters are listed in Sec. IV. Figures 5, 6, and 7 focus on the linear chain configuration (Fig. 1b) with nearest-neighbor couplings between chromophores. Figures 6 and 7 show the same quantities, but centered at different peaks ($\lambda \sim 450$ nm versus $\lambda \sim 513$ nm).

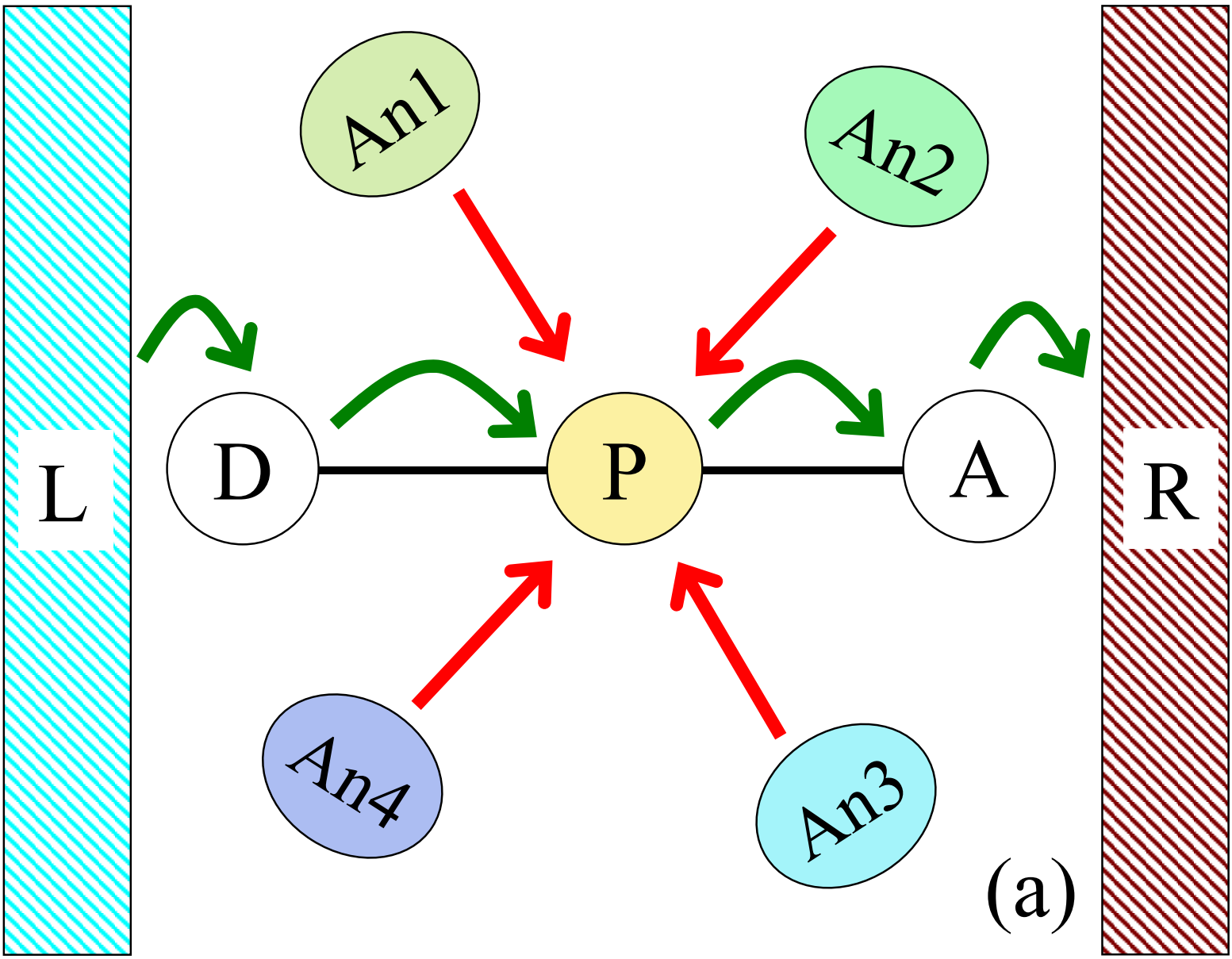

Figure 1a EJ10837 17Nov2011

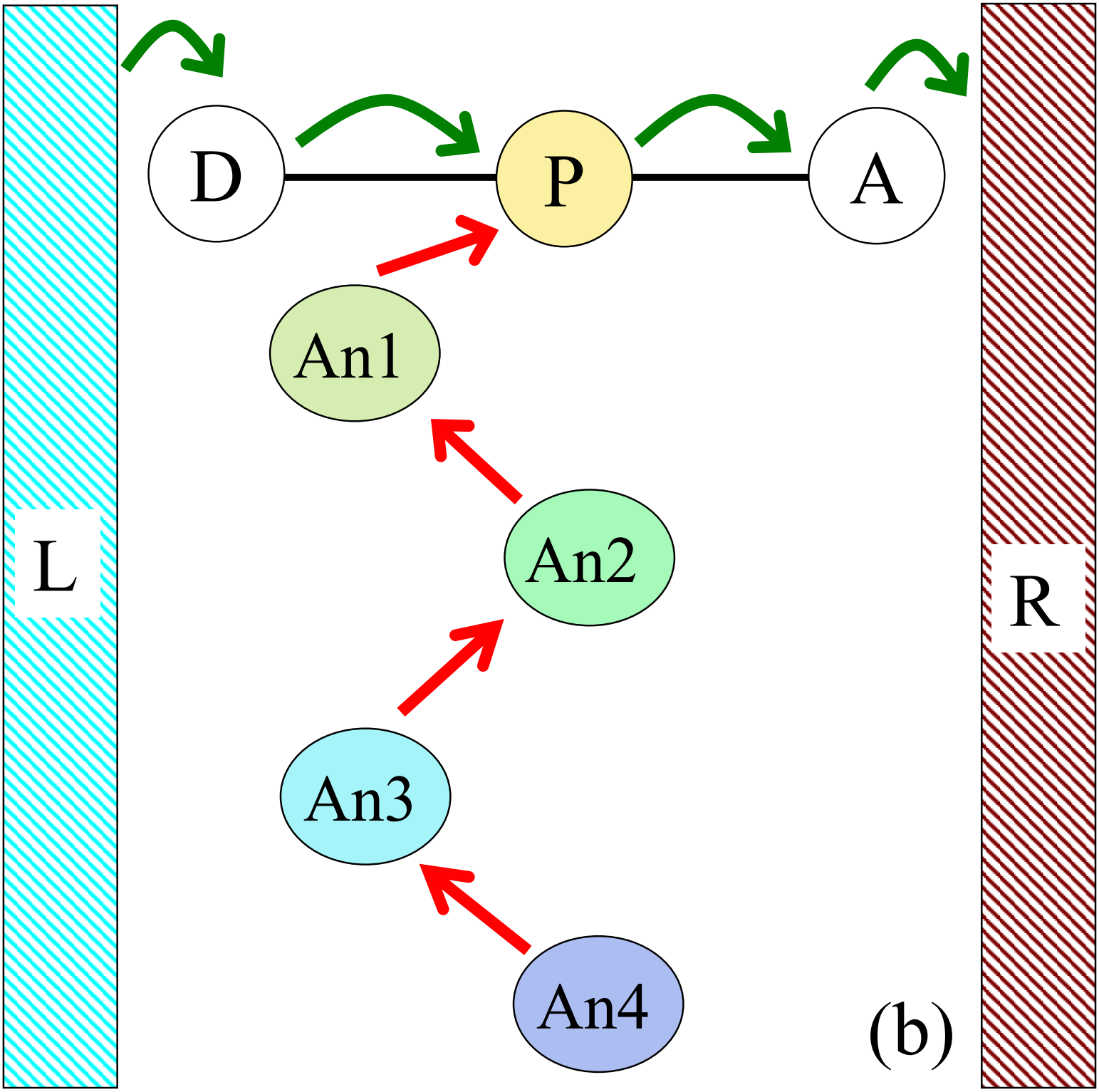

Figure 1b EJ10837 17Nov2011

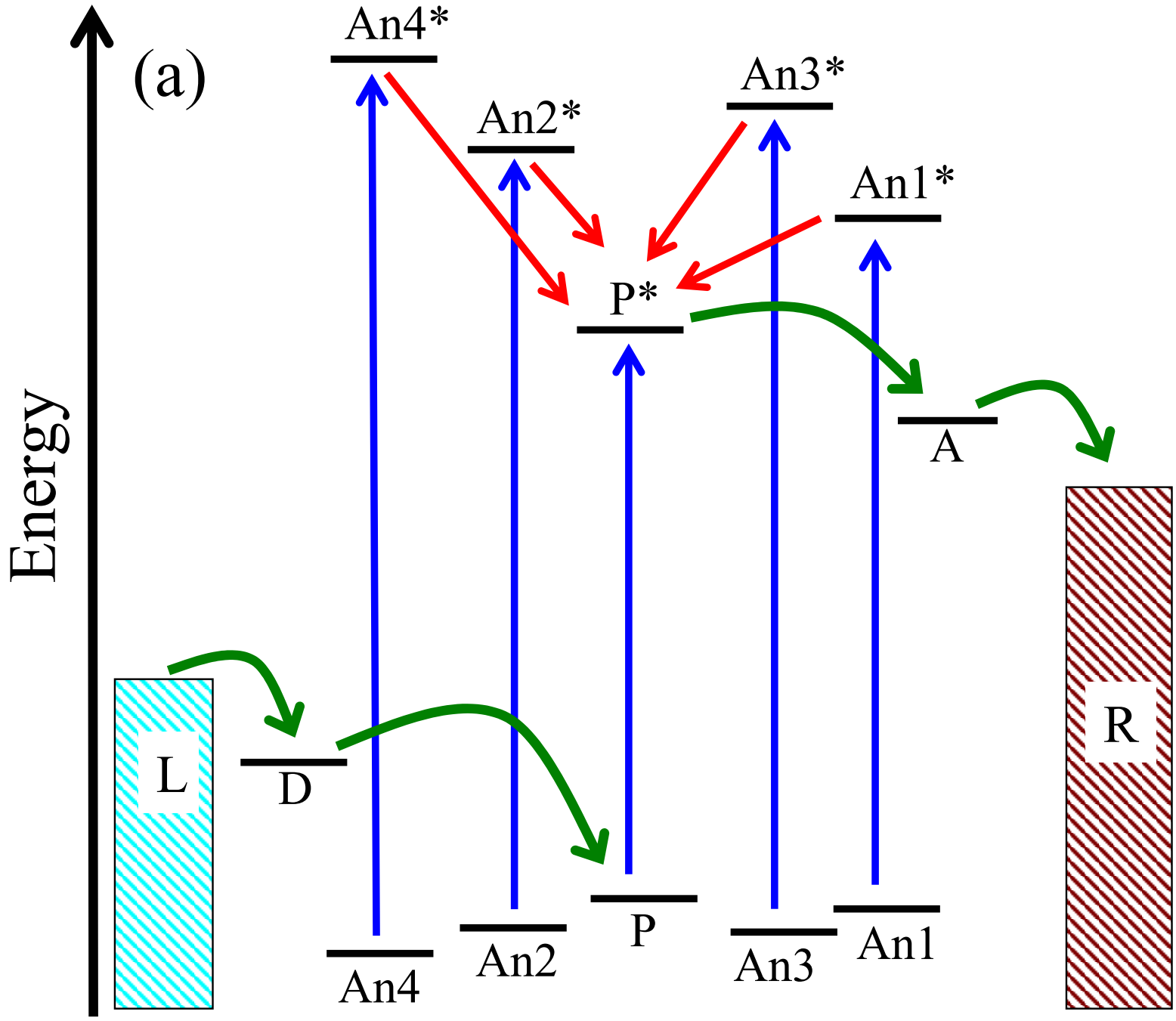

Figure 2a EJ10837 17Nov2011

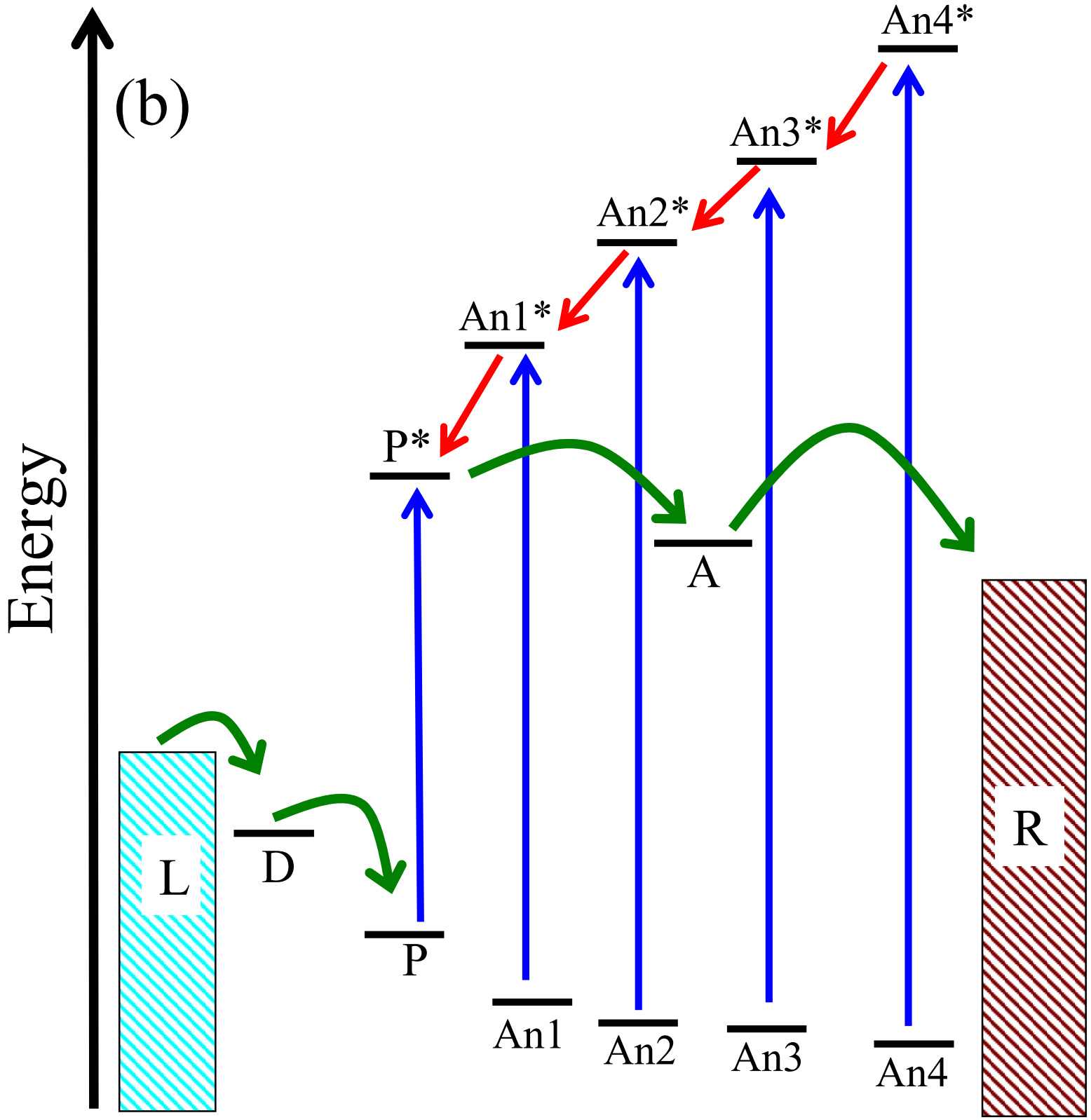

Figure 2b EJ10837 17Nov2011

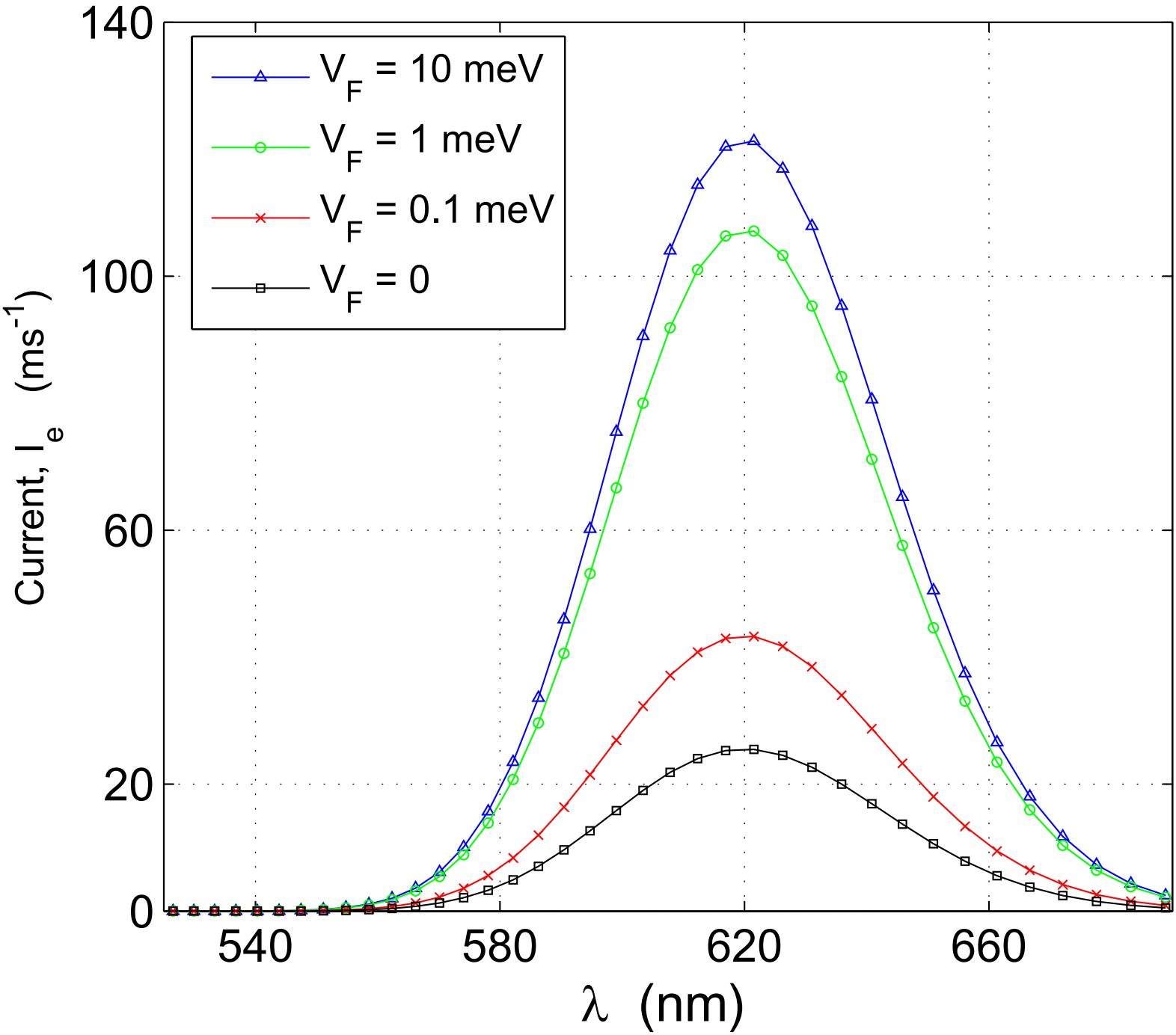

Figure 3 EJ10837 17Nov2011

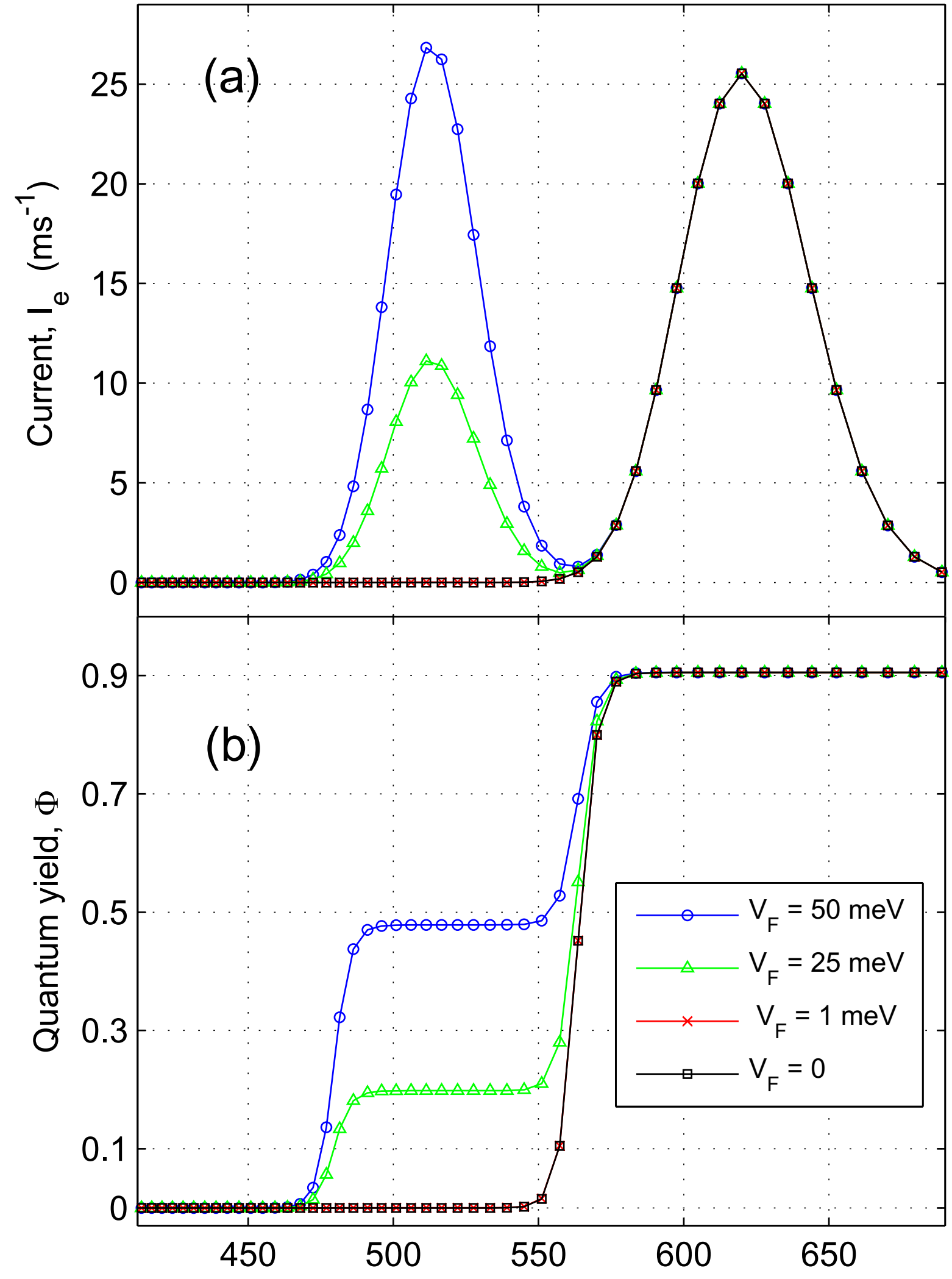

Figure 4 EJ10837(rm)17Nov2011

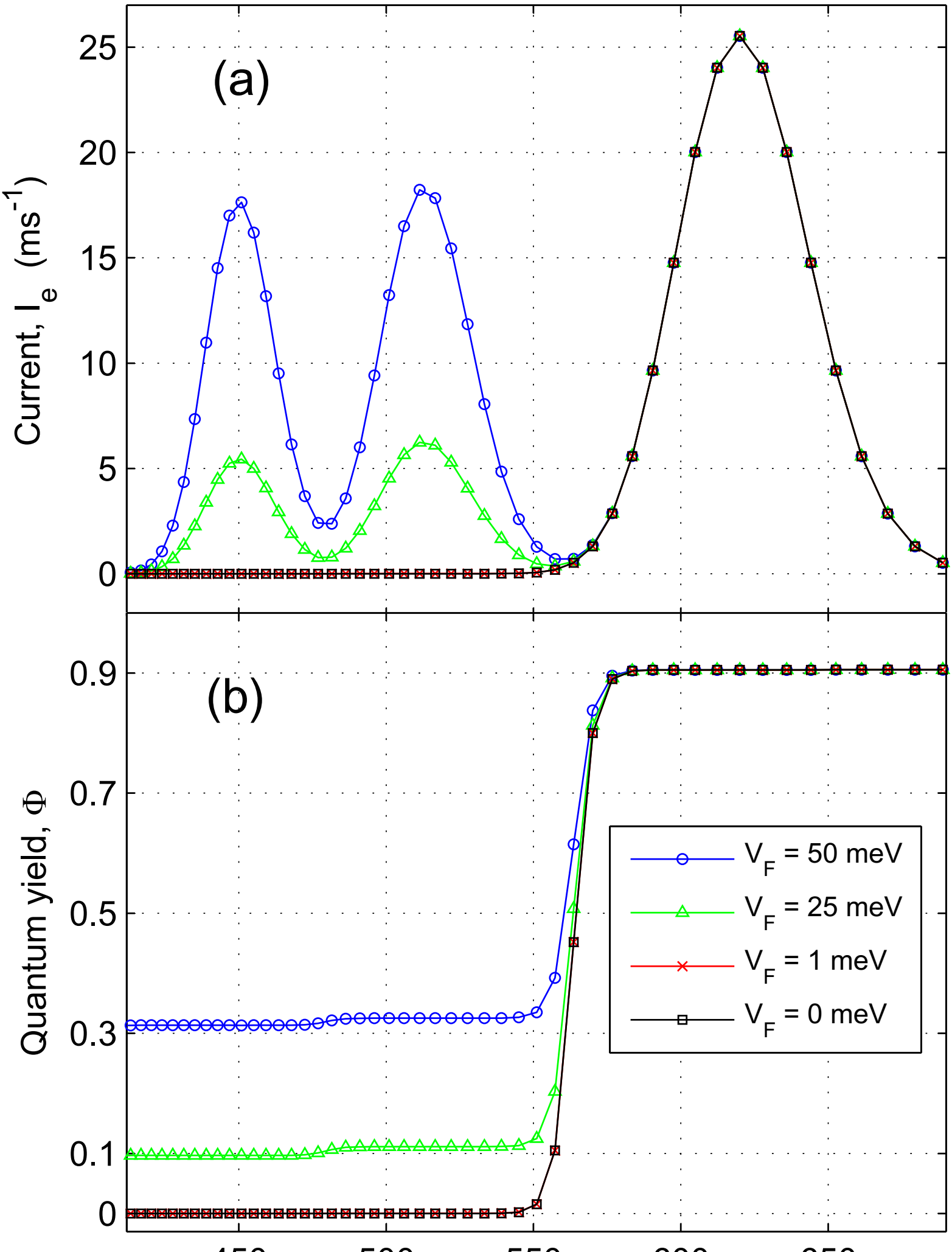

Figure 5 EJ1083(7) 17Nov2011

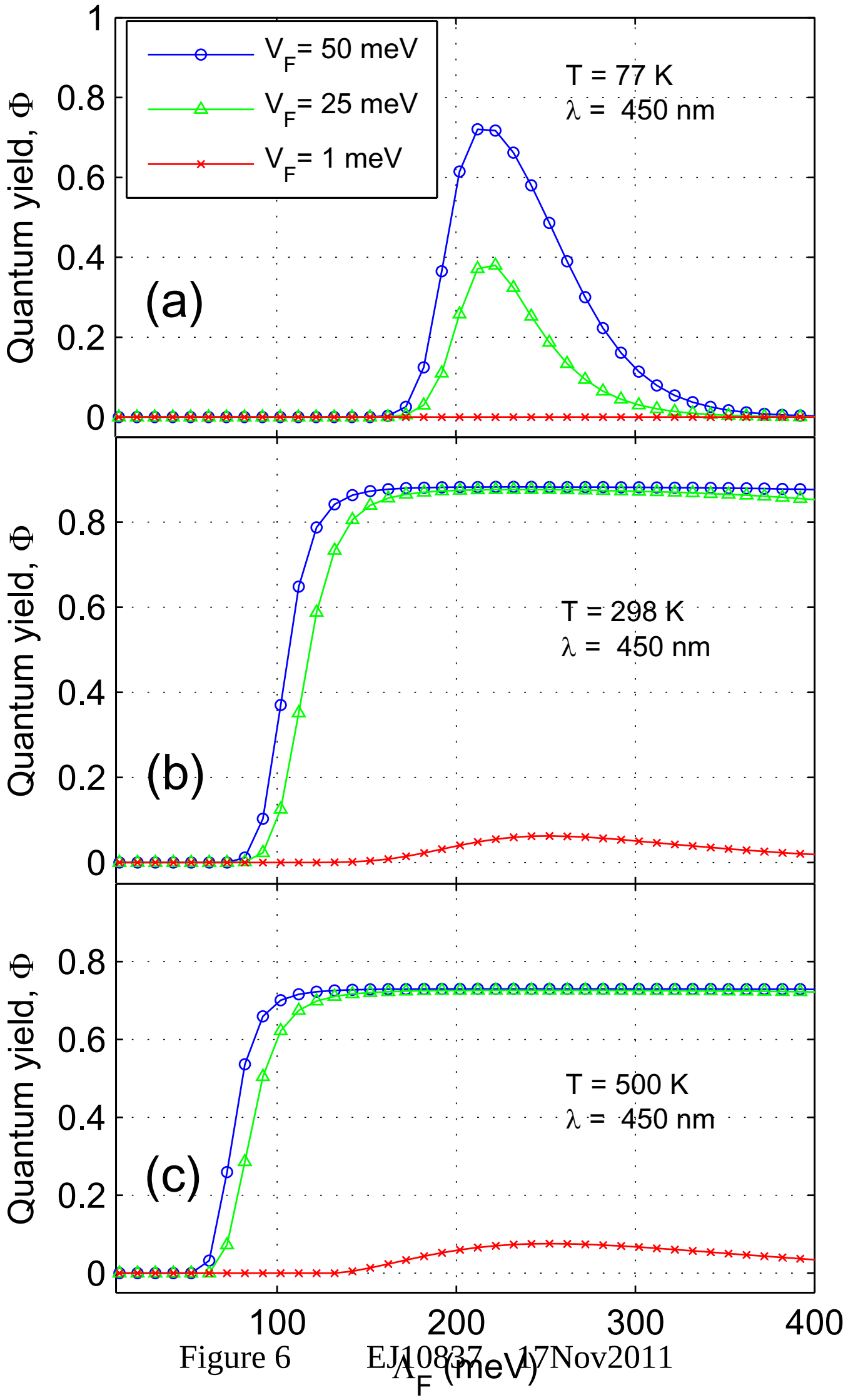

Figure 6 EJ10837_17Nov2011

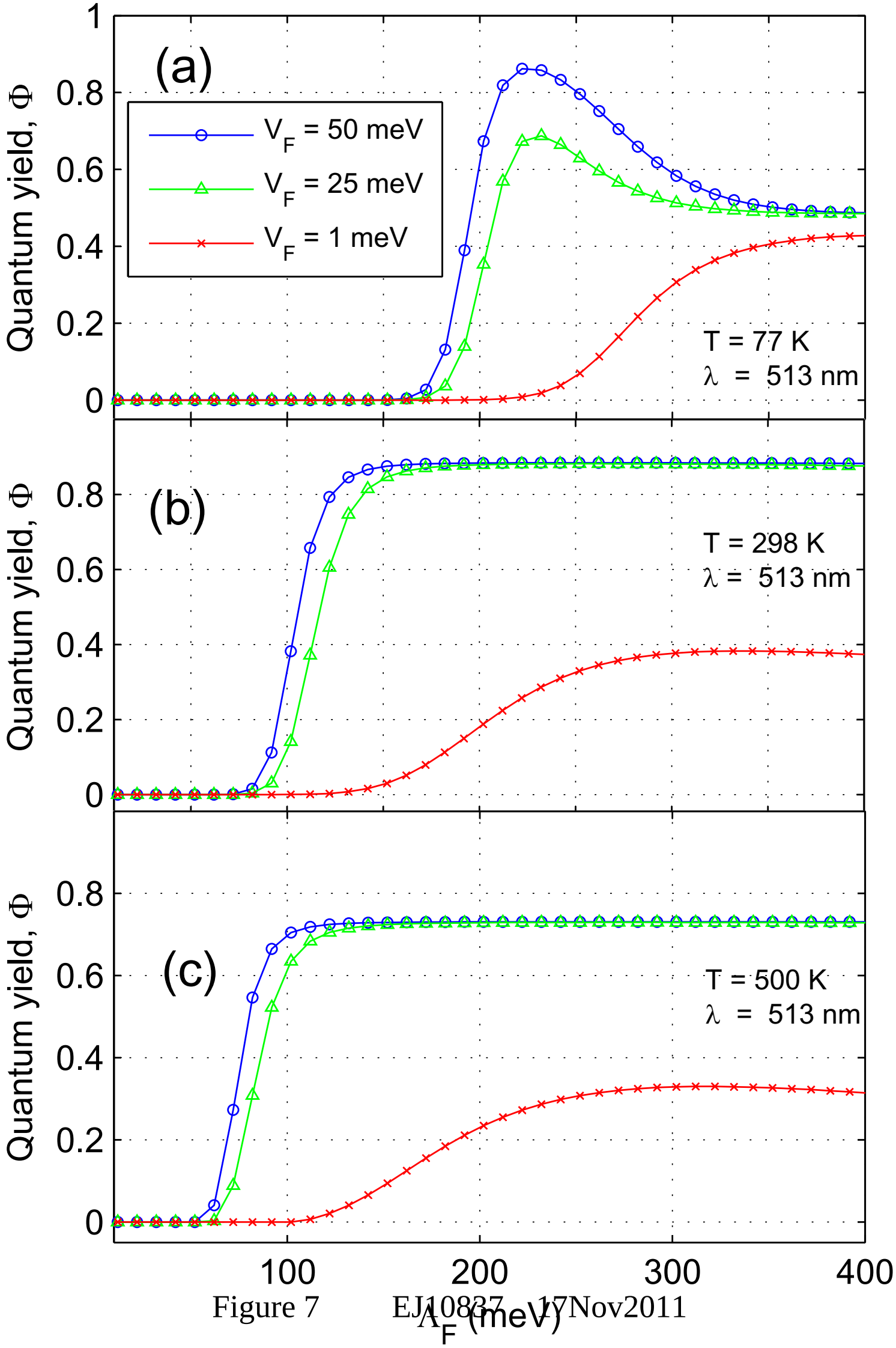

Figure 7 EJ10837 17Nov2011